Turbulence Modeling of JET SOL Plasma

V. Naulin[1], W. Fundamenski[2], A.H. Nielsen[1], J. Juul Rasmussen[1], O.E. Garcia[1], B. Gonçalves[3], C. Hidalgo[4], M. Hron[5], and JET-EFDA contributors[*]

[1] *Association EURATOM- Risø National Laboratory, OPL-128, 4000 Roskilde Denmark*
[2] *EURATOM/UKAEA Fusion Association, Culham Science Centre, Abingdon OX14 3DB, UK*
[3] *Associação EURATOM-IST, 1049-001 Lisbon, Portugal*
[4] *Associacion EURATOM-CIEMAT, Av. Complutense 22, 82040 Madrid, Spain*
[5] *Association EURATOM-IPP.CR, Prague, Czech Republic*
E-mail contact of main author: volker.naulin@risoe.dk

Abstract: The two dimensional (2d), electrostatic edge-SOL turbulence code ESEL is used to simulate the perpendicular dynamics of transport events in the JET Scrape Off Layer (SOL) and the self consistent development of the SOL profiles at the outboard midplane. The code results are compared to probe measurements of the JET SOL. Qualitative agreement is shown amongst others for profiles, for the magnetic field direction independent part of the parallel flow, and the correlation between parallel and perpendicular velocity fluctuations. The code predict magnetic field independent parallel flows with velocities of 0.2 ion sound speed The prospect of performing similar simulations for ITER is discussed.

1. Introduction

Understanding and modeling radial plasma transport originating at the transition from closed to open field lines is of vital importance for the development of fusion machines. The strongly intermittent turbulent transport fuels the Scrape Off Layer (SOL) and dictates the density and temperature profiles across the SOL. It is further responsible for plasma contact with the vessel wall, which is detrimental for the operation of fusion reactors as it not only damages plasma facing components, but will lead to an increased influx of impurities into the core plasma due to main vessel recycling. Transport modeling for the SOL has in recent years made tremendous progress, but still struggles to include the effects of turbulent transport in the SOL with high levels of intermittency as reported from a large number of devices. We here present results of a simple model, the ESEL model, that can be run long enough in time and with sufficient spatial resolution to produce selfconsistently the fine scale turbulence together with the evolution of the profiles, on which we here concentrate, properties of the fluctuations will be reported elsewhere.

2. The ESEL interchange model

Measurements of the ohmic L-mode SOL at JET and for a number of other devices show that the relative fluctuation levels of density $\tilde{n}/n$, temperature $\tilde{T}/T$, and of electrostatic potential fluctuations compared to the electron temperature $e\tilde{\phi}/T_e$ are of order unity, while magnetic fluctuations $\tilde{B}/B$ scale four orders of magnitude smaller. While this does not rule out a magnetic flutter contribution to the radial (r or x direction) transport, it characterizes the turbulence in the SOL as being dominated by electrostatic motions. Opposed to the turbulence inside the Last Closed Flux Surface (LCFS), which is found to be of the drift Alfvén type, measurements and 3d numerical simulations [1], indicate that the nature of the turbulence in the SOL is mainly of the flute mode type. This motivates us to model the SOL turbulence with an electrostatic 2d

[*] *[*]See the Appendix of M. L.Watkins et al., Fusion Energy 2006 (Proc. 21st Int. Conf. Chengdu, 2006) IAEA, (2006).*.

approach, where the parallel dynamics is reflected by losses of plasma, heat and polarization charge along magnetic field lines towards the divertor or limiter. The observed high fluctuation levels in the SOL and the significant variation in parameters across the SOL demand a global approach to the modeling, including the interaction between turbulent transport and the profiles and the variation of parameters with local plasma conditions. We restrict our approach to the dynamics at the outboard midplane, where interchange type instabilities are strongest [2] and as recently confirmed experimentally at Tore Supra [3] most of the transport into the SOL occurs. The equations in 2d slab geometry read:

$$\frac{dn}{dt} + n\kappa(\phi) - \kappa(nT) = D_{\perp n}\nabla^2 n - \frac{n}{\tau_{\|n}} + S_n$$

$$\frac{dT}{dt} + \frac{2T}{3}\kappa(\phi) - \frac{7}{3}T\kappa(nT) - \frac{2}{3}\frac{T^2}{n}\kappa(n) = D_{\perp T}\nabla^2 T - \frac{T}{\tau_{\|T}} + S_T$$

$$\frac{d\omega}{dt} - \kappa(nT) = D_{\perp\omega}\nabla^2\omega - \frac{\omega}{\tau_{\|\omega}} + S_\omega .$$

All quantities are normalized using the Bohm scaling with the characteristic time being the ion gyro frequency $\omega_{ci} = eB_0 / m_i$. Lengths are measured in multiples of the ion gyro radius at electron temperature $\rho_s = c_s / \omega_{ci}$. We emphasize that the model assumes cold ions for simplicity, a condition that is clearly not fulfilled in the SOL where the ion temperature often exceeds the electron temperature due to faster parallel heat loss of the electrons.

The total time derivative contains the electric drift as an advecting velocity. The vorticity is related to the curl of the velocity field and expressed as $\omega = \nabla_\perp^2 \phi$. Finally the curvature operator $\kappa(\cdot) = -\xi\partial y$ is given via the magnetic field variation $B(r) = 1/(1 + r_0 / R_0 + \xi r)$.

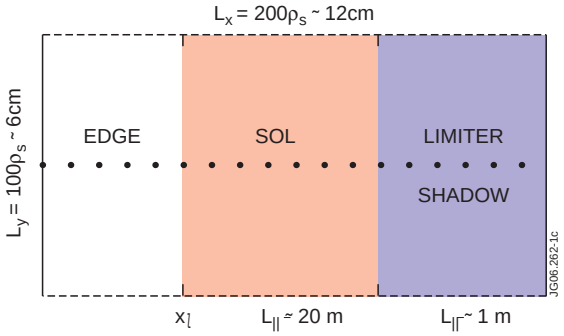

FIG. 1: Geometrical setup of the simulations

The parallel loss times are related to the parallel connection length $L_\| = \pi R_0 q_{95}$ unless the magnetic field lines end on wall limiter structures, where we replace $L_\|$ with the actual connection length from the outboard midplane to the wall limiter. For parallel density and vorticity losses we use the following expression

$$\tau_{\|\omega} \approx \tau_{\|n} = L_\| / M\xi c_s \propto 1/\sqrt{T_e} .$$

We regard the turbulent fluctuations at the outer midplane to be not in contact with the divertor plates. Thus the loss of vorticity is due to the parallel expansion of the structures once they enter the SOL, and not regulated by the sheath potential, as is often assumed, but directly proportional to the polarization charge what results in qualitatively and quantitatively different losses [2].

The parallel heat loss is given by the Spitzer-Härm diffusion in the collisional limit

$$\tau_{\|T} = 3/2 \;\; L_\|^2 / \chi_{\|e}^{SH} \propto n / T_e^{5/2} .$$

For the perpendicular diffusion terms we use neoclassical Pfirsch-Schlüter values reflecting the influence of the geometry on collisional transport, ν_{ab} being the collision frequency between species *a* and *b*:

$$D_{\perp n} = (1+1.3q_{95}^2)(1+\frac{T_i}{T_e})\rho_e^2\nu_{ei} \propto \frac{n_e}{\sqrt{T_e}}$$

$$D_{\perp \omega} = (1+1.6q_{95}^2)\ 3/8\ 2\rho_i^2\nu_{ii} \propto \frac{n_e}{\sqrt{T_i}}$$

$$D_{\perp T} = (1+1.6q_{95}^2)\left(4.66\rho_e^2\nu_{ee} + 2\rho_i^2\nu_{ii}\ 1/\left[1+\left(\frac{\nu_{e.\varepsilon}^*}{L_\parallel \nu_{ei}/\nu_{te}} \right)^2 \right] \right).$$

The coupling between electron and ion heat diffusivities is taken into account via the equipartition collisionality $\nu_{e,\varepsilon}^* = \sqrt{3.2/3\ m_i/m_e} \approx 64$ [4]. As the collisional terms vary with $n/\sqrt{T}$, which is roughly a constant in experiments as well as in the simulations, the radial variability of the diffusion coefficients was neglected in the simulations and the LCFS values are used.

It is worthwhile to note that in 3d self-consistent simulations the smaller classical values would have to be used instead of the neoclassical ones, as the neoclassical Pfirsch-Schlüter mechanisms should be a part of any self consistent 3d simulation which also includes evolution of the profiles [5]. The equations where solved on a numerical grid of 1024 times 512 points, corresponding to approximately 5 points per ρ_s. In time the simulations were run to extremely long times (corresponding to about 10ms at a timestep of 0.01 μs) to allow development of the profiles and to provide good statistics.

3. Requirements in modeling JET and larger devices

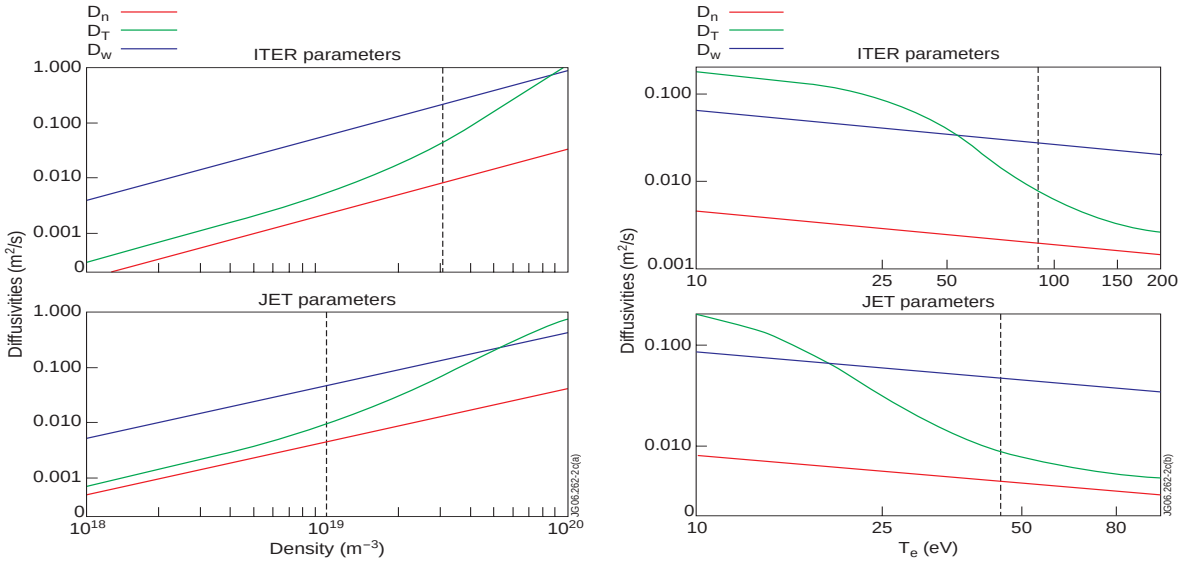

FIG. 2: Diffusion parameters as function of density (left column) and temperature (right column) for ITER (top) and JET (bottom). Parameters from table 1 are indicated.

Using the neoclassical values for the diffusive terms has shown to be important in obtaining good agreement with experimental values. It is instructive to see the variability of the coefficients with density and temperature, as is depicted in FIG. 2. Specifically, it is interesting to

note the transition in the relative importance of the heat diffusivity from being dominated by the coupling to the ions at high collisionality to be due to the electron-diffusion at low collisionality. The comparison between JET and ITER shows that the collisional effects in the SOL are much reduced for the hotter ITER machine. As the needed numerical resolution scales roughly inversely with the diffusion coefficients the overall computational demand for similar simulations at ITER parameters will be a factor of more than ten higher. Thus even such relatively straight forward 2d calculations will be demanding for ITER parameters.

	$n_{e,0}$	$T_{e,0}$	$T_{i,0}$	B_0	q_{95}	$L_\parallel$	$L_{\parallel wall}$	R_0	Δ_{SOL}	$\rho_{s,0}$	$\Delta_{SOL}/\rho_{s,0}$
JET	10^{19} m^{-3}	45 eV	80 eV	1.5 T	2.7	25.5 m	1 m	3 m	6 cm	0.64 mm	90
ITER	$3\ 10^{19}$ m^{-}	90 eV	160 eV	3.3 T	3.0	58.9 m	??	6.2 m	6 cm (??)	0.1 mm	600

Table 1: Basic parameters for JET [6] (pulses 50418 and 50420) and ITER, needed as input parameters in ESEL

4. Measurements of profiles

Plasma profiles and turbulence have been measured in the JET plasma boundary region Both plasma profiles and turbulence have been investigated using a fast reciprocating Langmuir probe system that consists of arrays of Langmuir probes allowing the simultaneous investigation of the radial structure of fluctuations and parallel Mach numbers. Plasma fluctuations were investigated using 500 kHz digitisers. The Mach number has been computed as $M=0.4\ ln(I^{ct}/I^{co})$ where I^{co} and I^{ct} represent the ion saturation current measured at each side of the Mach probe (i.e. co and counter direction magnetic field) [7]. Plasmas studied in this contribution were produced in X-point plasma (forward and reversed toroidal field) in ohmic L-mode regimes with toroidal magnetic fields B = 1.5 T and plasma current Ip = 2 MA. In addition measurements with Li beams were used for the profile comparisons. It should be noted, however, that the JET reciprocating probe is located nearly at the top of the tokamak vessel, implying a significant distance along the magnetic field lines from the outer midplane, where the simulations are applying, to the measurement point.

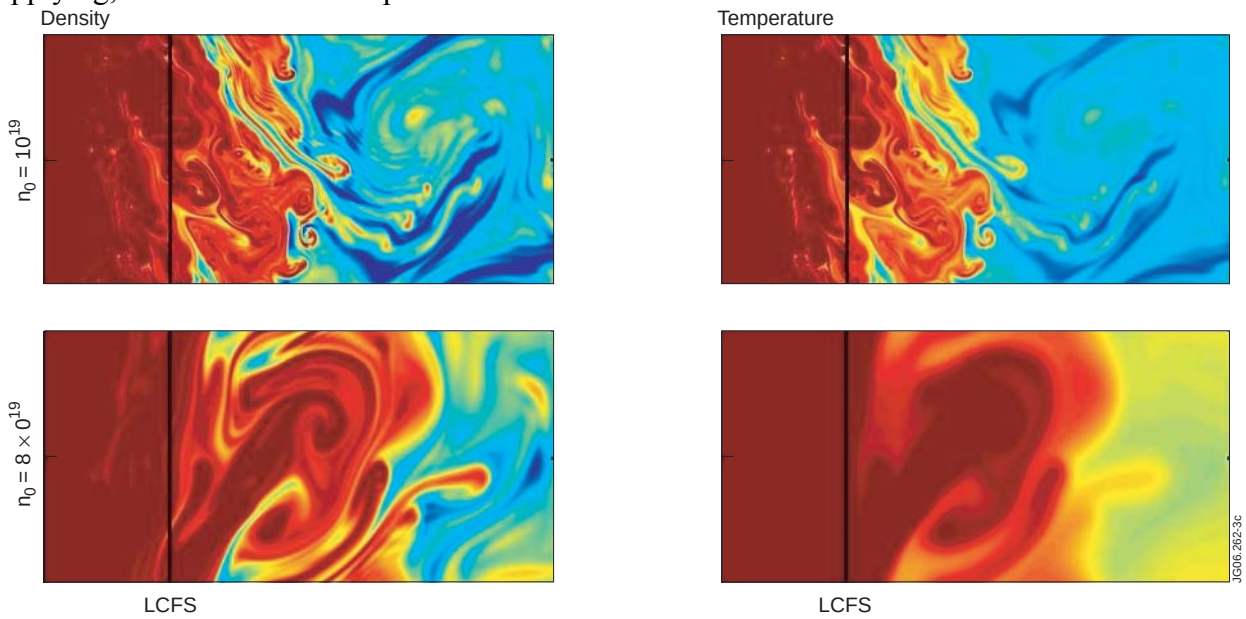

FIG. 3: Density and temperature fields for low and high collisionality.

5. Fluxes and profiles

The simulations produce a distinct different behavior in the edge and SOL region with a self consistently developing shear flow separating the two. Diffusive inflow into the edge region from the inner boundary fills up the edge with hot plasma. We should note that the model does not try to simulate the dynamics in the edge region, but that this edge region acts as a reservoir to fill in the SOL. At distinct times bursts of hot plasma evolve at the LCFS and send propagating blob structures deep into the SOL region where they loose energy and particles due to the parallel loss mechanisms. This bursty transport dominates over the inter blob transport. The radial velocity of the blobs in the simulations is about 5 percent of the ion sound speed, such that radial transport and parallel streaming with the ion sound speed are competing on the relevant length scales $L_{\|} / c_s \approx \Delta_{SOL} / V_{Blob}$ what a posteriori justifies the assumption of the blob filaments not being connected to the limiter/divertor plates.

One of the prominent signatures of the simulations is the strong dependence of the temperature dynamics on collisionality as can be seen from the snapshots of density and temperature shown in Figure 3**.** At high collisionality the fine structures in the temperature have nearly vanished. It should be noted that numerical codes which run with artificially increased dissipative terms will show similar behaviour.

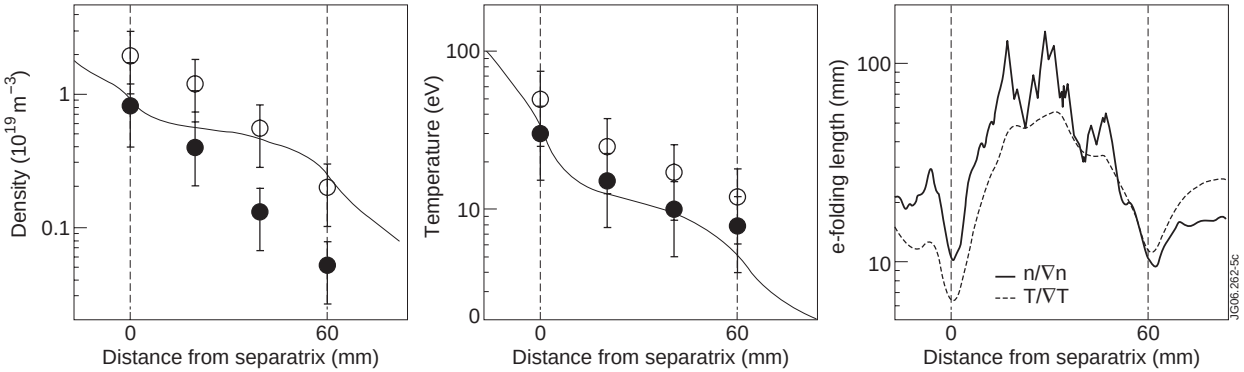

FIG. 4: Density and temperature profiles from the ESEL simulation compared to two measured profiles by Li-beam and probe measurements for shot no. 56891 (from [6]). Right the e-folding length showing the typical increase slightly outward the LCFS.

The resulting density and temperature profiles, shown in Figure 5 indicate a stronger decay of the density profile closer to the separatrix than further outwards. Steeper density profiles reflect the

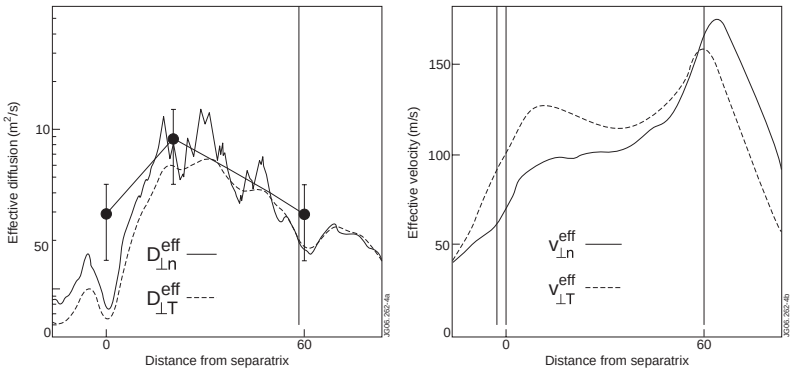

FIG. 5: Left: Effective diffusion coefficient from ESEL simulation compared to EDGE2D modeling of the plasma (dots with errorbars). Right: Effective convective velocities.

faster loss of particles to the divertor compared to electron energy. The overall behavior of the profiles from these first simulations compare reasonably well to experimental observations, where e-folding length values λ_n^{SOL} = 10-20 mm and λ_{Te}^{SOL} = 20 mm in the near SOL rising to more than 25-30 mm in the far SOL have been measured [6] in Ohmic limiter shots. The simulations produce profiles of density and temperature similar to the ones inferred from the experiments. As the profiles in the SOL are set up by the turbulence ejected at the LCFS an equivalent formulation is to look at the local effective diffusion coefficients $D_{\perp n}^{eff} = \Gamma / \langle \nabla_r n \rangle$ and $D_{\perp T}^{eff} = q/(n_0 \langle \nabla_r T \rangle)$ or, alternatively at the effective radial convection velocities $V_{\perp n}^{eff} = \Gamma / \langle n \rangle$ and $V_{\perp T}^{eff} = 2/5\ q / \langle n \rangle \langle T \rangle$. Both the effective diffusivities and convective velocities at the outer midplane, including the effects of both collisional and turbulent perpendicular transport, are shown in FIG. 5. The diffusivities increase from the separatrix to a peak value located at about 20 mm into the SOL, in qualitative and quantitative agreement with experimental observation [8]. While the effective diffusion varies by an order of magnitude over the SOL the effective convective velocities change only by about a factor two. It seems that this reflects a trend that in general the transport through the SOL seems to be better expressed in terms of the much less varying effective velocities [9], even though possibly neither effective diffusion coefficients nor effective velocities reflect the true nature of the intermittent transport in the SOL [10].

6. High field side to low field side coupling

To study the influence of blobs expanding along magnetic field lines to the high field side, we investigated an extension of the ESEL model, where two drift planes, one on the low field side and one on the high field side where coupled, by allowing density to flow between them. This allows density structures originating on the LFS to set up turbulence on the intrinsically stable high field side (HFS) which forms a variant of the turbulence spreading idea [11]. The turbulence created on the HFS is shown for this coupling to induce a net flux of heat and particles towards the core at a level that can be exceeding the neoclassical transport, a phenomenon often needed in 2d SOL modeling. This obviously occurs, when the density perturbation mapped to the HFS along magnetic field lines polarizes due to curvature and sets up a dipolar potential structure that convects it to lower magnetic field strength, i.e. radially inwards. If, on the other hand, the polarization charge mapping from the LFS should be the dominant mechanism for the potential generation on the HFS, a radial outward motion of the blobs would result, but at an reduced speed [12]. As, however, the strength of the coupling cannot be established from a 2d simulation, this effect calls for 3d simulations of the SOL turbulent transport to investigate its relative size.

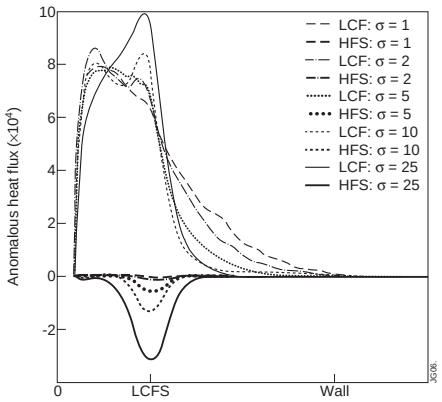

FIG 6: Inward transport induced on the LFS and HFS at different strengths of the parallel coupling between HFS and LFS density and normalized to the neoclassical transport values.

7. Parallel velocity

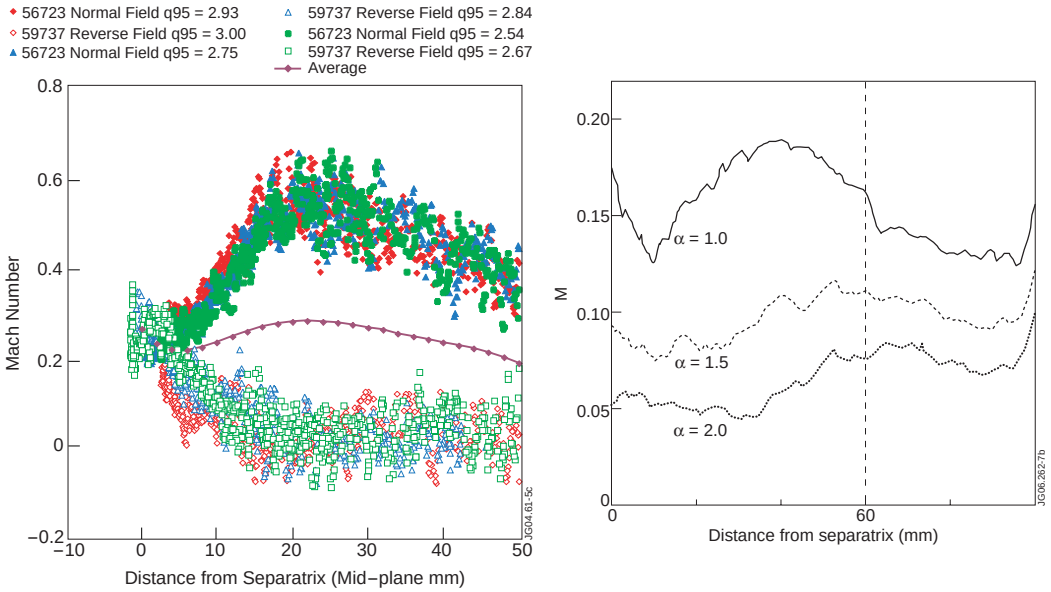

FIG 7: Measured parallel Mach number profile by reciprocating probe near top of the JET vessel (reproduced from [6]) and corresponding parallel velocity profile inferred from ESEL simulations for three values of α , to be compared with the average value in the left figure. Note the difference in radial extend.

Using Mach probes a strong $\mathrm{B}\times\nabla B$ independent parallel flow component has been observed on several machines, including JET. About the nature of this flow little is yet know besides its strong ballooning nature, even though the magnetic field dependent part of the parallel flow is thought to origin in the Pfirsch-Schlüter return flow. We infer the parallel flow velocity from the 2d ESEL simulations by assuming that the blob structures have a finite parallel extend and create a parallel pressure gradient which is the cause of the parallel flow. We therefore estimate the local Mach number via $\langle M \rangle \approx 0.5\, f_{p>\alpha\langle p\rangle}$ with $f_{p>\alpha\langle p\rangle} \equiv \int dt\; t(p > \alpha \langle p \rangle / \Delta t$ that is we relate the average flow to the time the local pressure exceeds it background value. Ideally the free parameter α should be close to unity. The ESEL simulations for JET predict parallel Mach numbers M ~ 0.2 for the $\mathrm{B}\times\nabla B$ independent part of the parallel flow in agreement with Mach probe measurements for $\alpha = 1$ as shown in FIG 7. Also the slight rise inward from the LCFS is captured. Comparison of the parallel Reynoldsstress, as shown in FIG. 8, is in fair agreement between simulation and experiment [13], with an increase in the correlation further from the LCFS into the SOL, which can be interpreted as being due to the dominance of filament structures causing likewise radial and parallel velocity fluctuations.

8. Conclusions

We have performed simulations of the JET SOL with the Risø ESEL model. Very high numerical resolution is required for the emerging quantitative agreement with experimental data. In addition the position of the reciprocating probe at JET, close to the top of the vessel, makes a direct comparison with turbulence calculated at the outer midplane difficult. Nevertheless we demonstrate that the model can reproduce not only the qualitative aspects of the SOL turbulence, but also quantitative ones.

Specifically the simulations give a reasonable agreement with observed profiles at JET, suggest an explanation for the magnetic field independent part of the parallel flow velocity, the profile of the parallel momentum transport, and could indicate the presence of a small heat flux into the main vessel on the HFS triggered by the turbulence transported from the LFS to the HFS.

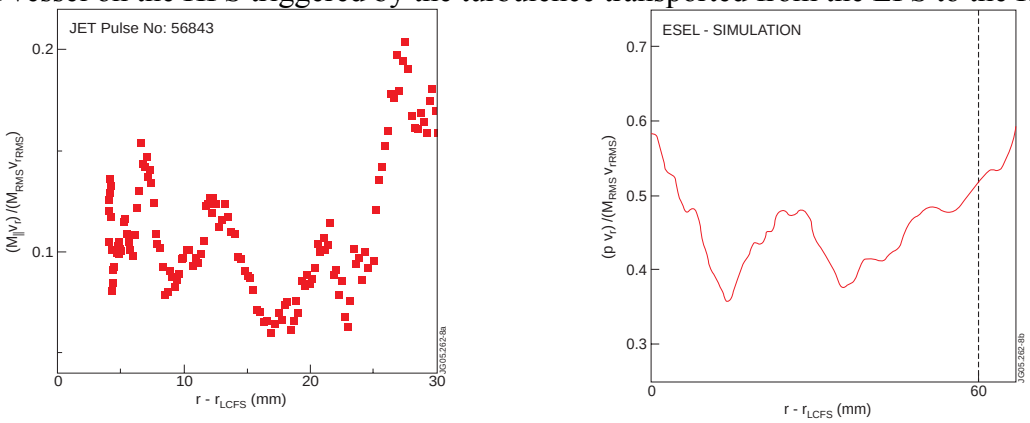

FIG. 8: Correlation between parallel and radial velocity fluctuations, experiment (left) [13] and simulations (right).

On the basis of the reasonable agreement between simulation and experiment we conclude that the SOL radial transport in JET ohmic plasmas is dominated by electrostatic interchange turbulence characterized by radially propagating blobs, with the ratio of blob velocity to parallel losses setting the profiles, as has also been clearly revealed for the smaller TCV device [2]. In these blob dominated situations the average effective convective velocity can be linked to the blob speed and the density of the blobs.
Future work will be concerned with the extension of the model to include finite ion temperature effects, estimates of recycling and impurity influxes from the wall, and finally a 3d extension of the code.

Acknowledegements:

The work was supported through the Danish Centre for Scientific Computing. OEG was supported with financial subvention from the Danish Agency for Science, Technology and Innovation.

[1] *T. Ribeiro and B.D. Scott, Plasma Phys. Control. Fusion, 47, (2005), 1657*
[2] *O.E.Garcia et al., Phys. Plasmas 12 (2005) 062309, O.E. Garcia et al., Plasma Phys. Control Fusion 48 (2006) L1, J. Horacek et al., EX/P4-21, 21th IAEA Conference, Chengdu, China, 2006*
[3] *J. Gunn et al., J. Nucl. Mat. 2006 (in print)*
[4] *W. Fundamenski et al., submitted to Nucl. Fusion (2006)*
[5] *B. D. Scott, private communication*
[6] *K.Erents et al., Plasma Phys. Control Fusion 46 (2004) 1757*
[7] *I.H. Hutchinson, Phys. Rev. A, 37 (1988), 4358*
[8] *K. Erents et al., Nuclear Fusion 38 (1998) 1637*
[9] *W. Fundamenski et al., submitted to Plasma Phys. Control. Fusion 2006*
[10] *V. Naulin, J. Nucl. Materials 2006 (in print)*
[11] *T.S. Hahm et al., Plasma Phys. Control. Fusion 46(2004) A323 , V. Naulin et al., Phys. Plasma 12, (2005), 122306*
[12] *G.S. Kirnev et al., Nuclear Fusion 45 (2005) 459*
[13] *B. Goncalves et al., Proceedings of the 20th IAEA Conference, (Vilamoura, Portugal 1-6 November 2004)*